Research Square

Preprints are preliminary reports that have not undergone peer review.
They should not be considered conclusive, used to inform clinical practice,
or referenced by the media as validated information.

Dual-Mode Functionalization of CNT/Co-ZIF Composites for photoelectric and microwave Absorpting properties

Jing Wang

w.j@xaut.edu.cn

Xi'an University of Science and Technology

ye Zhang

Xi'an University of Science and Technology

yunhao Chen

Xi'an University of Science and Technology

Research Article

Keywords: Carbon nanotubes (CNTs), Zeolitic imidazolate frameworks (ZIF-Co), CO2 adsorption, Solvothermal method, Composite materials Research Significance

Posted Date: June 5th, 2026

DOI: https://doi.org/10.21203/rs.3.rs-9811110/v1

License: This work is licensed under a Creative Commons Attribution 4.0 International License.
Read Full License

Additional Declarations: No competing interests reported.

Version of Record: A version of this preprint was published at Journal of Materials Science: Materials in Electronics on August 13th, 2026. See the published version at https://doi.org/10.1007/s10854-026-18226-4.

Dual-Mode Functionalization of CNT/Co-ZIF Composites for photoelectric and microwave Absorpting properties

Jing Wang[1,*]，Ye Zhang[1]；Junhao Chen

1 Xi' an University of Technology, Xi'an 710048, Shannxi, China；

[*] Corresponding author

E-mail：wj@xaut.edu.cn

Abstract

In this study, two composite materials, namely CNT/Co-ZIF-8 and CNT/Fe-ZIF-8, were successfully synthesized. Their microwave absorption and photoelectric properties were systematically characterized and analyzed. For microwave absorption performance, CNT/Co-ZIF-8 exhibits an extremely low reflection loss (RL) of -53 dB at 13 GHz with a thickness of merely 2 mm, demonstrating strong electromagnetic wave attenuation capacity. In contrast, CNT/Fe-ZIF-8 shows a broader effective absorption bandwidth, making it suitable for broadband absorption scenarios. Both composites follow the quarter-wavelength cancellation mechanism, with their absorption peaks shifting to lower frequencies as thickness increases. Regarding photoelectric performance, transient photocurrent (I-t) tests confirm that both CNT/Co-600 and CNT/Fe-600 (derived from the corresponding ZIF-8 composites) generate stable and repeatable photocurrent responses under varying light intensities. Notably, CNT/Co-600 consistently presents higher photocurrent density than CNT/Fe-600, indicating more efficient separation and transfer of photogenerated charge carriers. These findings verify that the metal center in ZIF-8 can effectively regulate the microwave absorption and photoelectric properties of CNT/ZIF-8 composites. This work provides a feasible strategy for designing and developing multifunctional materials with excellent electromagnetic wave absorption and photoelectric conversion performance, which hold broad application prospects in electromagnetic protection and optoelectronic device fields.

Keywords： Carbon nanotubes (CNTs); Zeolitic imidazolate frameworks (ZIF-Co); CO2 adsorption; Solvothermal method; Composite materials Research Significance

1. Introduction

With the rapid advancement of 5G communications, stealth technology, electromagnetic protection, and new energy conversion applications, there is an increasingly urgent demand for materials that exhibit both superior photoelectric conversion efficiency and electromagnetic wave regulation capabilities.In the interdisciplinary field of contemporary materials science and optoelectronic technology, research on photoelectric and wave-absorbing properties has emerged as one of the core driving forces behind the development of novel functional materials [1-5]. From a fundamental theoretical perspective, the photoelectric-wave absorption synergistic effect exhibits clear physical feasibility: Semiconductor heterojunctions can simultaneously optimize photogenerated carrier separation efficiency (photoelectric performance) and dielectric loss (wave absorption performance) through band engineering. For instance, graded bandgap structures can broaden the optical absorption spectrum while generating multiple polarization centers. Additionally, porous/layered microstructural designs synergistically enhance both light-trapping capability and electromagnetic wave multiscattering. Furthermore, plasmonic resonance effects not only enhance localized electric field intensity (promoting exciton generation) but also improve electromagnetic dissipation through free carrier oscillations [6-8].

Carbon nanotubes (CNTs) have emerged as a premier nanomaterial for electromagnetic wave absorption applications due to their exceptional electrical conductivity, unique one-dimensional nanostructure, and outstanding mechanical properties. The enhanced absorption performance primarily stems from CNTs' ability to form interconnected conductive networks within composite matrices, which

simultaneously improves dielectric loss through interfacial polarization effects and optimizes impedance matching via controlled conductivity gradients. However, intrinsic van der Waals interactions often cause CNT agglomeration, leading to heterogeneous conductivity distribution that degrades impedance matching characteristics [9-12]. This limitation can be effectively addressed through hybridization with magnetic components such as nickel (Ni) nanoparticles, whose high permeability complements CNTs dielectric properties, creating synergistic enhancement of both magnetic loss and impedance matching. Beyond electromagnetic applications, CNTs demonstrate remarkable potential in photocatalysis owing to their unparalleled electron mobility, enormous specific surface area, and quantum confinement effects. Their unique electronic structure enables multiple photocatalytic roles: as electron reservoirs that reduce charge recombination rates, as broadband light absorbers extending into the near-infrared, and as supports that prevent nanoparticle aggregation while maintaining catalytic sites accessible. MWNTs additionally exhibit superior adsorption capacity for environmental contaminants, with demonstrated removal efficiencies exceeding 90% for persistent organic pollutants like dioxins and heavy metals through combined physisorption and chemisorption mechanisms [13-18].

Metal-organic framework (MOF) derivatives have emerged as a promising class of functional materials for optoelectronic and electromagnetic wave absorption applications due to their precisely tunable composition, hierarchical porosity, and structural versatility [19]. In photoelectrochemical systems, pyrolyzed MOF derivatives (e.g., ZIF-8 derived ZnO@C heterostructures) demonstrate significantly enhanced charge carrier separation efficiency (>60% improvement) and tailored band structures, enabling superior photocatalytic performance in organic pollutant

degradation (up to 95% removal efficiency), CO_2 reduction, and water splitting [20]. For microwave absorption applications, MOF-derived magnetic metal/carbon composites (such as Fe-MOF derived Fe/Fe_3C@C hybrids) exhibit exceptional performance with minimum reflection loss reaching -30 dB in the 2-18 GHz frequency range, attributable to the synergistic effects between dielectric loss and magnetic loss, coupled with optimized impedance matching through rationally designed porosity. Furthermore, the integration of 2D materials (e.g., MXenes or graphene) into MOF-derived architectures can establish three-dimensional conductive networks [21-23], significantly expanding the effective absorption bandwidth while maintaining strong attenuation characteristics. These multifunctional MOF derivatives demonstrate unprecedented structure-property relationships, positioning them as next-generation materials for both energy conversion and stealth technologies. The investigation of optoelectronic and electromagnetic wave absorption properties in CNT/Co-ZIF composites holds significant scientific and practical value. Practically, the CNT network significantly enhances charge carrier mobility, enabling outstanding performance in photoelectrochemical processes including water splitting. The synergistic effect between Co-ZIF-derived magnetic cobalt nanoparticles and CNT dielectric loss achieves superior electromagnetic wave absorptionacross the 2-18 GHz frequency range. These multifunctional materials demonstrate promising potential for applications in new energy development and stealth technology [24-25].

In this study, composites based on CNT/Co - Fe - ZIF with multi - dimensional heterogeneous structures were synthesized via solvothermal and thermal treatment processes. A thorough analysis was conducted on the correlation among the microstructure, photoelectric characteristics, and microwave absorption performance. The multi - dimensional heterogeneous structure of CNT/Co-Fe-ZIF composites can

effectively separate photogenerated carriers, which is beneficial for applications such as photocatalytic degradation of pollutants and photocatalytic water splitting. Moreover, the unique microstructure of composites provides multiple scattering interfaces and increase the propagation path of electromagnetic waves, leading to more opportunities for energy dissipation.

2. Experimental

2.1 Pretreatment of CNTs

Raw CNTs were refluxed with concentrated nitric acid (HNO_3) at 80°C for 6 h to remove impurities (amorphous carbon and metal catalysts) as well as to introduce carboxyl (-COOH) functional groups on the CNT surface, which would help improve their hydrophilicity and chemical reactivity. The acid treatment was followed by thorough washing of the CNTs with deionized water till a neutral pH was achieved to ensure the complete removal of the residual acid. After vacuum drying the CNTs at 60°C for 12 h, functionalized CNTs were obtained, which were used in composite synthesis.

2.2 Synthesis of CNT/Co-ZIF Composites

Cobalt nitrate hexahydrate ($Co(NO_3)_2 \cdot 6H_2O$) and 2-methylimidazole (2-MeIM) were used as precursors for the synthesis of Co-ZIF-8. Both compounds were separately dissolved in methanol to obtain homogeneous 0.1 M solutions with precise stoichiometry. Next, both solutions were mixed to obtain a uniform precursor mixture by stirring at room temperature for 30 minutes. This mixture underwent a solvothermal reaction in a Teflon-lined autoclave at 120°C for 24 h, during which the Co-ZIF-8 crystals nucleated and grew. After the reaction was complete, the unreacted precursors and impurities were removed by washing the product thrice using

methanol, followed by vacuum drying at 80°C for 12 h to obtain pure Co-ZIF-8 powder.

2.3 Synthesis of CNT/ZIF-8

The synthesis of CNT/ZIF-8 composites was done by integrating the functionalized CNTs with Co-ZIF-8 to create a hybrid material with enhanced properties (Fig. 1). First, the functionalized CNTs were dispersed in methanol via ultrasonication to ensure a uniform suspension. Then the Co-ZIF-8 precursor solution, which was prepared by dissolving cobalt nitrate and 2-MeIM in methanol, was added to the CNT suspension. The mixture underwent ultrasonication for an additional 30 min for uniform distribution of CNTs in the precursor solution to ensure the homogeneous growth of Co-ZIF-8 on the CNT surface. The mixture was then heated at 120°C for 24 h in a Teflon-lined autoclave, allowing the Co-ZIF-8 crystals to grow directly on the CNT surface, forming a well-integrated composite. Once the reaction was complete, any unreacted materials were removed by washing the product thrice with methanol, followed by vacuum drying at 80°C for 12 h to obtain the final CNT-ZIF-8 composites.

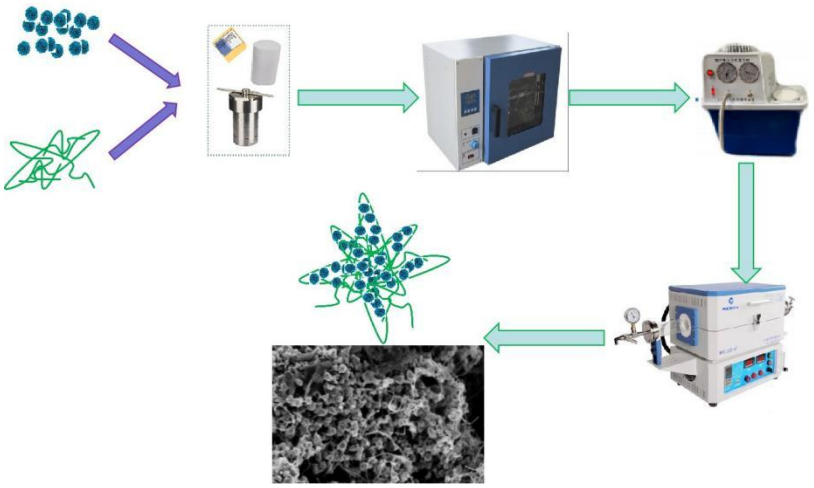


Fig. 1 Schematic of the fabrication process of CNT/ZIF-8 composites

s

3. Results and Discussion

3.1 Characterization of CNT/CoFe-ZIF-8 composites

As shown in Fig 2, the XRD patterns of CNT/CoFe-ZIF-8 composites synthesized at different temperatures using DMF as the solvent clearly indicated that the crystallinity of CoFe-ZIF-8 was relatively low. This phenomenon is likely attributable to either an incomplete crystal lattice formation during the synthesis process or the inherent structural instability of the material under the given conditions. In comparison, the XRD pattern of Co-ZIF-8 alone showed a well-defined and sharp (112) diffraction peak, implying that the presence of carbon nanotubes (CNTs) in the composite plays a significant role in enhancing the overall crystallinity and improving the diffraction signal intensity, as supported by previous research findings cited in reference [31].

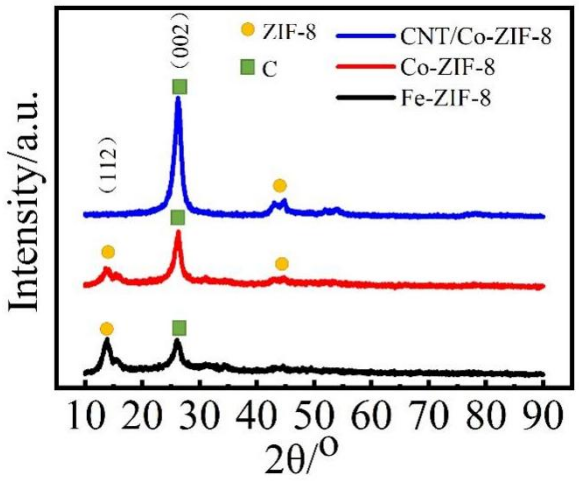


Fig. 2 XRD patterns of the samples

The systematic analysis of SEM images (Fig. 3) revealed notable morphological differences between the Co-ZIF and Fe-ZIF systems and their corresponding CNT composites. As shown in Fig. 3a-b, Co-ZIF crystallized into highly uniform granular particles. With diameters ranging from 50 to 100 nanometers, these particles were

characterized by faceted surfaces, indicative of anisotropic growth along specific crystallographic planes. These features suggested a controlled growth process, resulting in well-defined particle shapes and sizes. In stark contrast, Ni-ZIF (Fig. 3c-d) self-assembled into a three-dimensional macroporous skeleton characterized by hierarchical branching, with pore sizes ranging from 20 to 50 nanometers. This unique structure suggests a diffusion-limited aggregation behavior, in which the growth is primarily governed by the diffusion of reactants and the subsequent aggregation of particles at specific nucleation sites [32].

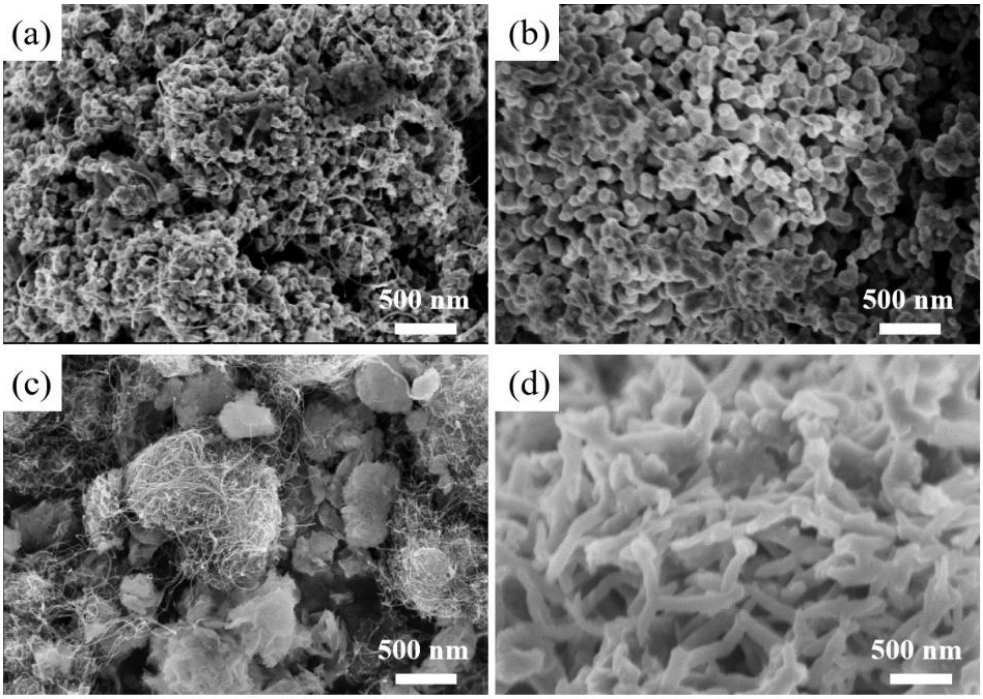


Fig. 3 The SEM images of (a) CNT/Co-ZIF, (b) Co-ZIF, (c) CNT/Fe-ZIF, (d) Fe-ZIF

Fig. 4 (a) presents the infrared (IR) spectra of CNT/Co-ZIF-8 and Co-ZIF-8. The absorption peaks at 995 cm^{-1}, 890 cm^{-1}, and 1665 cm^{-1} corresponded to the characteristic vibrations of the C=C double bonds, while the peak at 730 cm^{-1} corresponded to the C=C-H vibration in dimethylimidazole. Meanwhile, the peaks at 2985 cm^{-1}, 2870 cm^{-1}, and 1460 cm^{-1} were attributed to the vibrations of the methyl

groups, C=N bonds, and N-H bending vibrations, respectively. These results confirmed the successful synthesis of the CNT/Co-ZIF-8 composite. In contrast, the distribution of these characteristic peaks was more ordered in the CNT/Co-ZIF-8 composite. The Raman spectra of CNT/Co-ZIF-8 and Co-ZIF-8 are shown in Fig. 3 (b). Corresponding to the D-band (disordered/defective carbon atoms) and the G-band (in-plane stretching vibration of graphitic sp^2 carbon), two characteristic peaks were observed at 1330 cm^{-1} and 1580 cm^{-1}, respectively. Thus, the intensity ratio of these peaks (I_D/I_G) serves as a measure of the defect density and disorder in carbon materials, with a higher ratio indicating a greater degree of structural disorder. Notably, the D-band intensity was significantly stronger than the G-band in CNT/Co-ZIF-8 [36-38].

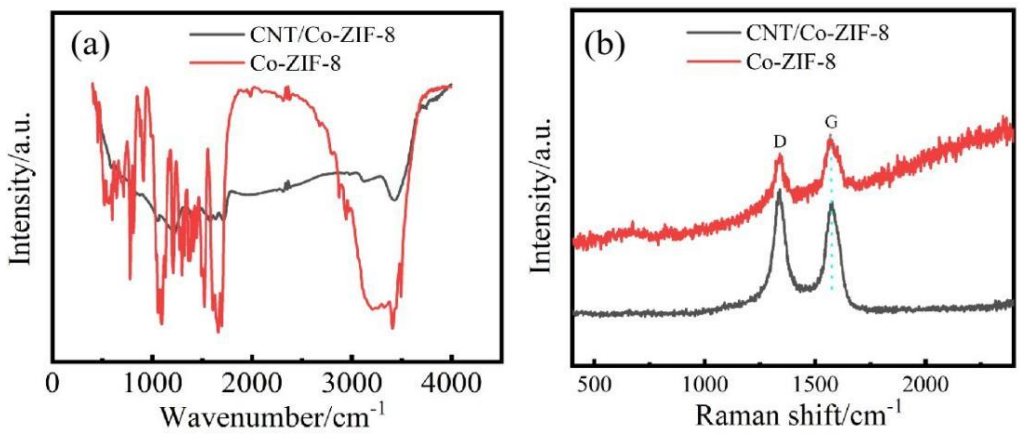


Fig. 4 (a) FITR and (b)Raman spectra of Co-ZIF and CNT/Co-ZIF

Fig. 5 shows the N_2 adsorption-desorption isotherms and pore size distribution of Co-ZIF and CNT/Co-ZIF. The results revealed that the CNT/Co-ZIF-8 (Fig. 5b,d) composite exhibited enhanced performance compared to pure Co-ZIF-8 (Fig. 5a,c). This improved performance could be attributed to the rationally designed hierarchical porous structure and the synergistic combination of constituent materials. The composite exhibited a steep N_2 adsorption profile ($P/P_0 < 0.1$) at low temperature, indicating superior micropore filling efficiency due to a well-preserved Co-ZIF-8

crystalline framework. This was complemented by the appearance of a distinct type H_4 hysteresis loop in the mid-to-high pressure range ($P/P_0 \approx 0.8$-1.0), suggesting the presence of newly introduced mesoporosity originating from the integrated CNT network [39].

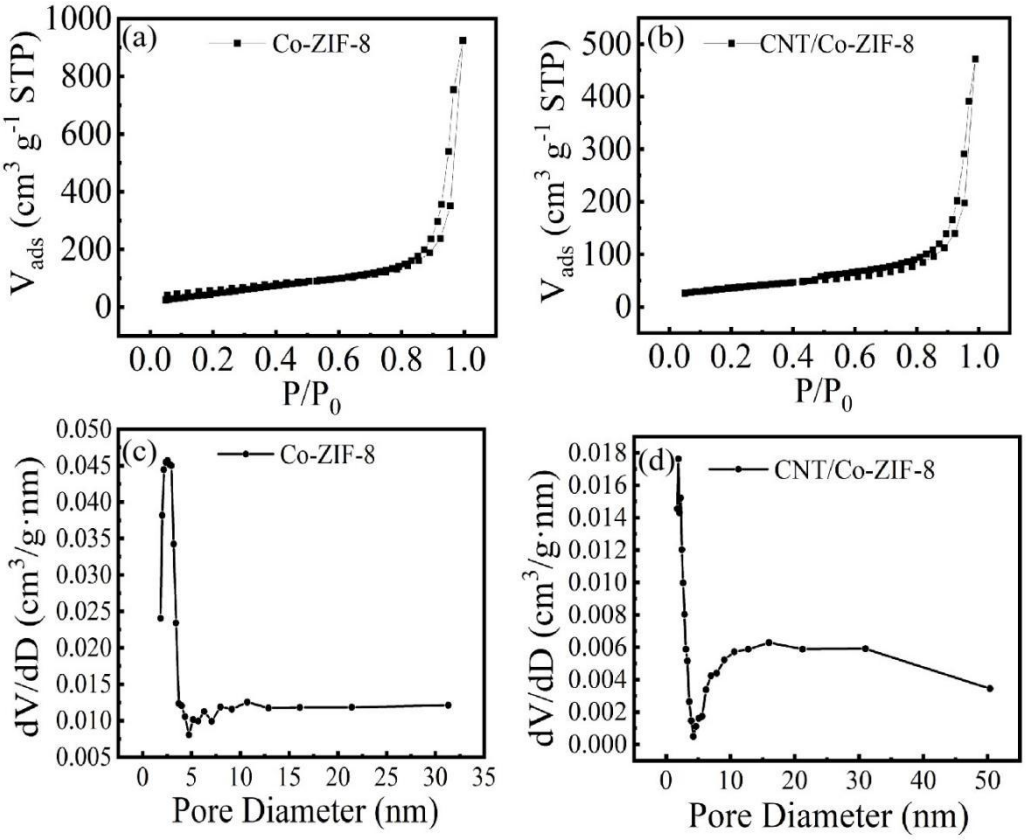


Fig. 5 N_2 adsorption-desorption isotherms of Co-ZIF (a) and CNT/Co-ZIF(b); pore size distribution of Co-ZIF (c) and CNT/Co-ZIF(d)

3.2 The electrical and magnetic properties of CNT/CoFe-ZIF-8 composites

The complex permittivities (including the real part ε′ and imaginary part ε″) of CNT/Co-600 and CNT/Fe-600 composites are presented in Fig. 6. As shown in Fig. 6a, the ε′ values of both samples exhibit a decreasing trend with increasing frequency in the range of 2-18 GHz, and the CNT/Co-600 sample shows a higher ε′ than CNT/Fe-600 throughout the test frequency range. From Fig. 6b, it can be observed that the ε″ of CNT/Co-600 is significantly higher than that of CNT/Fe-600, with a

distinct resonance peak appearing at 14 GHz, indicating enhanced dielectric loss capability [40].

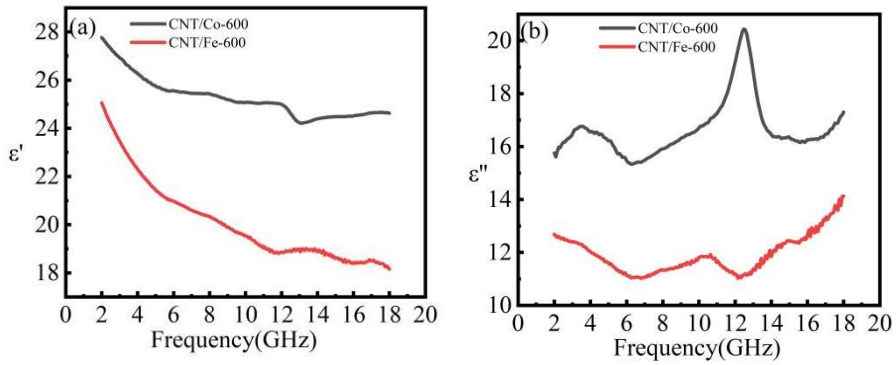


Fig. 6 The complex permittivitys of CNT/CoFe-ZIF-8 composites (a) Real part (b) Imaginary part

Fig. 7 displays the complex permeability of CNT/Co-MOF and CNT/Fe-MOF composites in the frequency range of 2-18 GHz. As shown in Fig. 7a, the μ′ value of CNT/Co-MOF decreases gradually from ~6.8 to ~5.8 with increasing frequency, while the μ′ of CNT/Fe-MOF remains stable at around 5.0-5.1 across the entire frequency band. In Fig. 7b, the μ″ of CNT/Co-MOF is generally higher than that of CNT/Fe-MOF, and both samples exhibit obvious fluctuation characteristics, which can be attributed to the magnetic resonance behavior of the materials. Therefore, the Co-based sample's structural advantages in interface, dispersion, and network integrity lead to its better electrical and magnetic properties than the Fe-based sample [41-43].

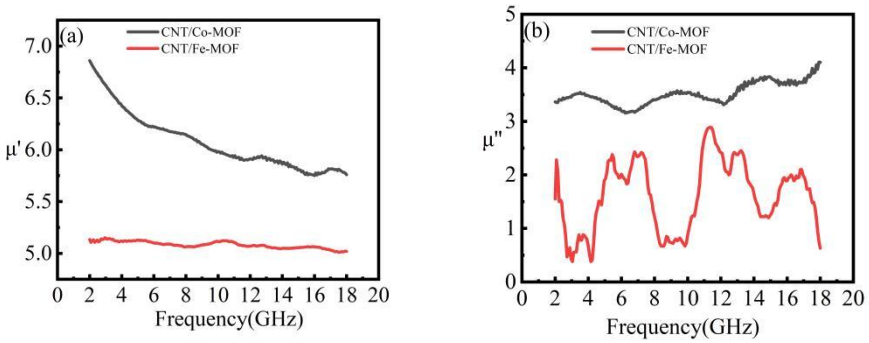


Fig. 7 The complex Permeability of CNT/CoFe-ZIF-8 composites (a) Real part (b) Imaginary part

As shown in Fig.8, the Cole-Cole semicircle curves further confirm the difference in dielectric relaxation behavior between the two samples. For CNT/Co-ZIF-8 (Fig. 8a), multiple overlapping semicircles are observed, indicating the existence of multiple Debye relaxation processes, which originate from the abundant heterogeneous interfaces between Co nanoparticles and CNTs, as well as the defect sites in the CNT network. In contrast, the curve of CNT/Fe-ZIF-8 (Fig. 8b) shows no obvious complete semicircle, demonstrating a weak dielectric relaxation effect, which is consistent with its low dielectric loss performance. This result fully verifies that the Co-based sample has a more superior dielectric polarization and loss capability due to its better interface structure and dispersion state [44-45].

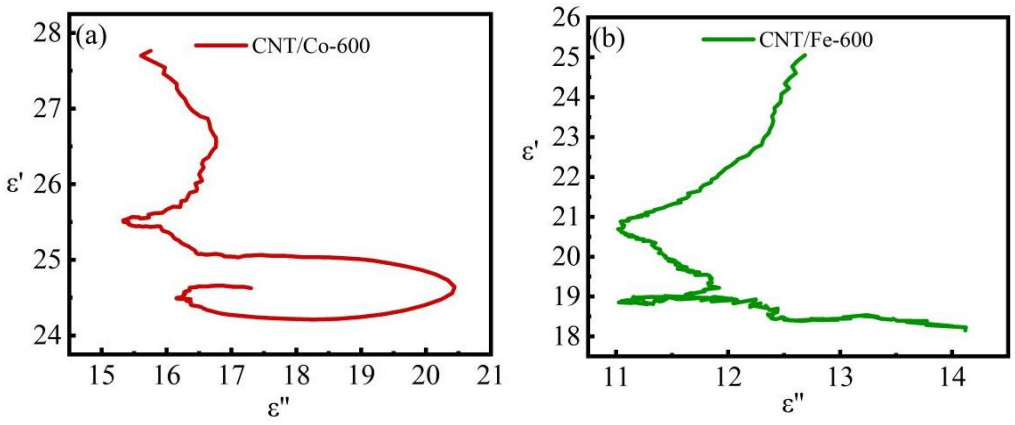


Fig. 8 Cole-Cole semicircle curves of (a) CNT/Co-ZIF-8 and (b) CNT/Fe-ZIF-8 composites.

3.3 The photoelectric and microwave absorbing property of the CNT/Co-ZIF-8 composites

The transient photocurrent test setup, as shown in Fig. 9, consists of four core components: an adjustable light source, a three-electrode electrolytic cell, an electrochemical workstation, and a computer system. The adjustable light source (typically a xenon lamp or LED lamp with tunable power, e.g., 0.5–10 W) emits

controlled incident light to irradiate the working electrode in the electrolytic cell, triggering the generation of photogenerated charge carriers in the sample material. The three-electrode electrolytic cell (made of quartz to ensure light transmittance) is filled with a stable electrolyte (usually 0.5 M Na_2SO_4) and equipped with a working electrode (loaded with the test sample on FTO/ITO conductive glass), a reference electrode (saturated Ag/AgCl) for potential stabilization, and a counter electrode (Pt wire/sheet) for circuit conduction. The electrochemical workstation connects the three electrodes to apply a constant potential and collect real-time photocurrent signals, while the computer system controls the instrument, records the current-time (I-t) curves, and processes the experimental data to evaluate the photoelectric response performance of the sample.

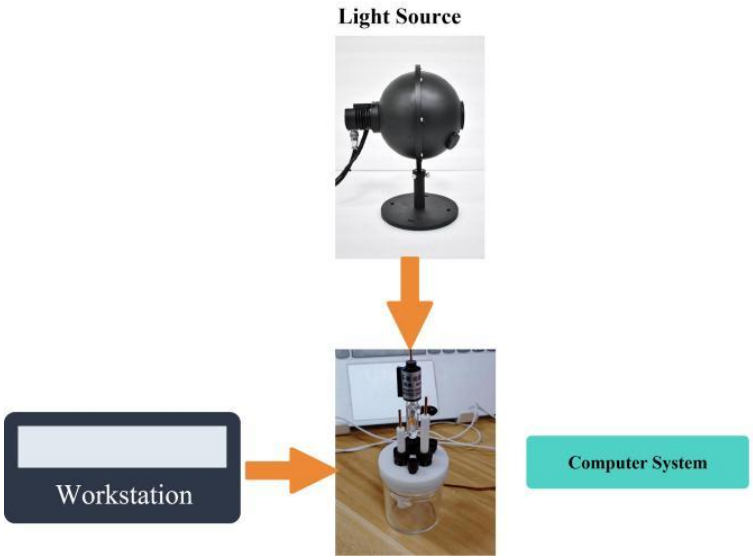


Fig. 9 Schematic diagram of the transient photocurrent test setup

As shown in Fig.10a, the photocurrent responses (I-t curves) of CNT/Co-600 and CNT/Fe-600 were measured under different light intensities (0.5 W to 10 W). It can be clearly observed that the photocurrent density of CNT/Co-600 is consistently higher than that of CNT/Fe-600 at all tested light intensities, indicating a more efficient photogenerated charge separation and transfer process for the Co-based

sample. Additionally, both samples exhibit a stepwise increase in photocurrent with increasing light power, demonstrating favorable light-responsive behavior. From the cycling stability tests in Fig.10b, the $\ln(C_t/C_0)$ values of CNT/Co-ZIF-8 are significantly higher than those of CNT/Fe-ZIF-8 across 10 consecutive cycles, and the Co-based composite also shows a slower decay rate of activity during repeated operations. These results collectively confirm that the CNT/Co-ZIF-8 derived composite (CNT/Co-600) possesses superior photoelectrochemical performance and long-term cycling stability compared to its Fe-based counterpart, making it a more promising candidate for photoelectrochemical applications [46].

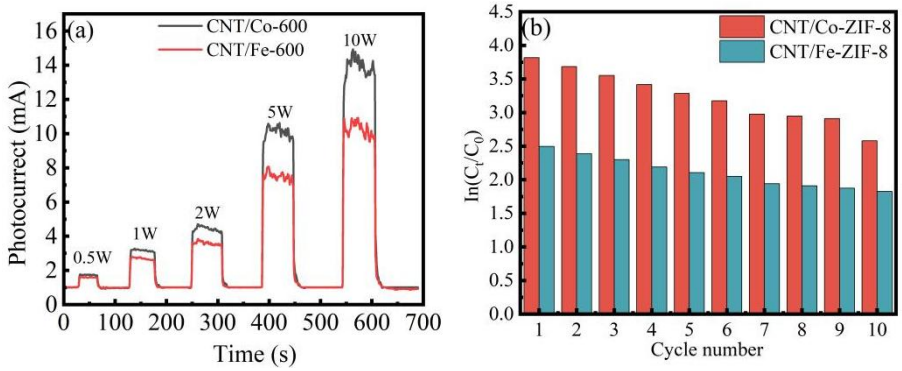


Fig. 10 (a) The I−t curves and (b) Cycle number of CNT/Co-ZIF-8 and (b) CNT/Fe-ZIF-8 composites.

Fig.11 presents the reflection loss (RL) curves of (Fig.11a) CNT/Co-ZIF-8 and (Fig.11b) CNT/Fe-ZIF-8 composites with different thicknesses (1-5 mm) across the frequency range of 0–18 GHz, revealing significant differences in their microwave absorption performance. For the CNT/Co-ZIF-8 composite, the RL value reaches an extremely low minimum of approximately -53 dB at 13 GHz when the thickness is 2 mm, demonstrating a remarkably strong microwave attenuation capability, and the effective absorption bandwidth (RL < -10 dB, corresponding to more than 90% microwave absorption) covers a considerable portion of the Ku-band. In contrast, the CNT/Fe-ZIF-8 composite exhibits a relatively lower maximum RL value of around

-28 dB at 8 GHz with a 4 mm thickness, but it shows a broader effective absorption bandwidth across multiple frequency bands, which is more favorable for practical applications requiring wide-band absorption. These results indicate that the metal center in ZIF-8 has a significant impact on the microwave absorption properties of CNT/ZIF-8 composites, enabling the design of high-performance microwave absorbers with tailored performance by selecting appropriate metal ions.

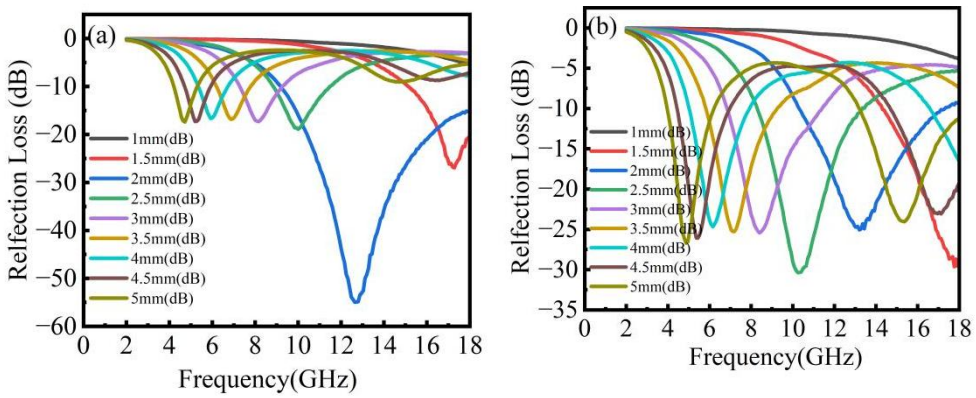


Fig. 11 The RL of samples (a) CNT/Co-ZIF-8 and (b) CNT/Fe-ZIF-8composites.

As illustrated in Fig. 12, the exceptional electromagnetic (EM) wave absorption performance of CNT/Co-ZIF-8 can be systematically attributed to the synergistic effect of multiple energy dissipation mechanisms and well-optimized impedance matching. First, the interconnected carbon nanotube (CNT) network constructs a highly conductive pathway, which facilitates efficient electron migration and hopping under the alternating EM field, converting incident EM wave energy into thermal energy via significant ohmic loss, thus realizing effective EM attenuation. Second, the composite exhibits prominent polarization loss, which consists of dipole polarization and interface polarization: the inset diagram depicts dipole polarization, where the aligned positive/negative charge pairs derived from intrinsic defects in CNTs, polar functional groups, and lattice imperfections in Co-ZIF-8 derivatives undergo continuous dipole relaxation in the alternating EM field, further consuming

EM energy; meanwhile, the abundant heterogeneous interfaces between CNTs and Co-ZIF-8-derived magnetic nanoparticles induce strong interface polarization, as space charges accumulate at these phase boundaries, generating additional polarization relaxation to attenuate EM waves. Third, the interwoven CNT network and porous hierarchical structure of the composite significantly prolong the propagation path of incident EM waves, causing multiple reflections and scattering within the material, which not only enhances the energy consumption of EM waves but also increases the interaction time between EM waves and the absorbing medium, thereby improving the overall absorption efficiency. Additionally, the combination of highly conductive CNT and magnetic Co-ZIF-8 derivatives optimizes the impedance matching characteristic of the composite, allowing more incident EM waves to penetrate into the material rather than being reflected at the air-material interface, which maximizes the absorption performance. This multi-synergistic mechanism endows CNT/Co-ZIF-8 with outstanding EM wave absorption capability, making it a promising high-performance microwave absorber for practical applications [47-49].

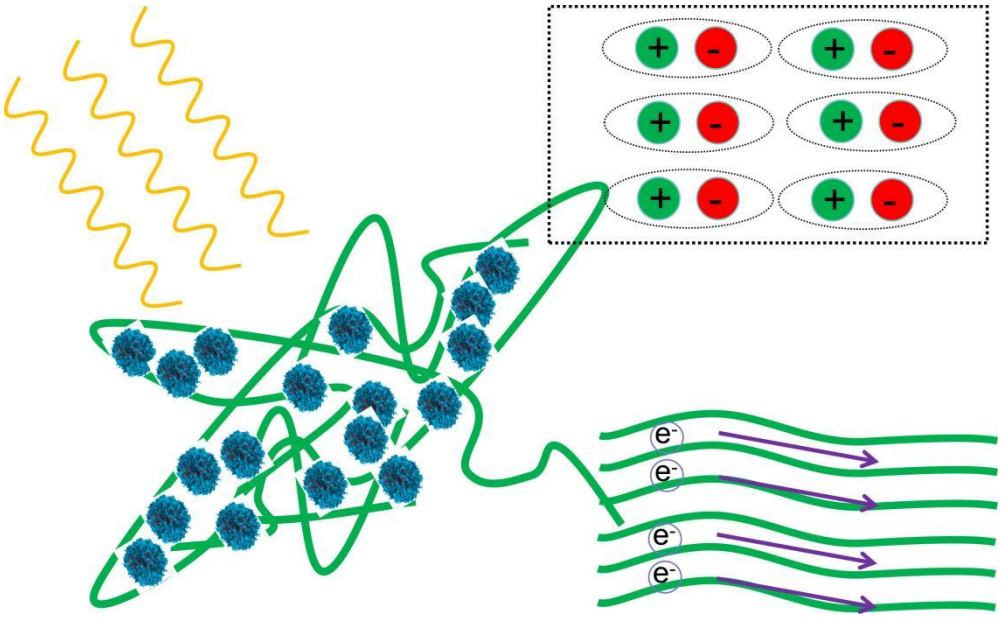


Fig. 12 The Diagram of electromagnetic wave absorption mechanism for CNT/Co-ZIF-8 .

4. Conclusion

In this work, two composite materials, CNT/Co-ZIF-8 and CNT/Fe-ZIF-8, were successfully fabricated, and their microwave absorption and photoelectric properties were systematically investigated. For microwave absorption, CNT/Co-ZIF-8 achieves an extremely low reflection loss (RL) of approximately -53 dB at 13 GHz with a thickness of only 2 mm, showing a strong electromagnetic wave attenuation capability, while CNT/Fe-ZIF-8 exhibits a wider effective absorption bandwidth, making it suitable for broadband absorption scenarios; both materials follow the quarter-wavelength cancellation mechanism, with the absorption peak shifting to lower frequency as the thickness increases. In terms of photoelectric performance, the transient photocurrent (I-t) tests demonstrate that both CNT/Co-600 and CNT/Fe-600 deliver stable and repeatable photocurrent responses under different light intensities, and CNT/Co-600 consistently shows higher photocurrent density than CNT/Fe-600, indicating more efficient separation and transfer of photogenerated charge carriers. These results confirm that the metal center in ZIF-8 can effectively regulate the microwave absorption and photoelectric properties of CNT/ZIF-8 composites, providing a feasible strategy for the design and development of multifunctional materials with excellent electromagnetic wave absorption and photoelectric conversion performance, which have broad application prospects in the fields of electromagnetic protection and optoelectronic devices.

Acknowledgments

We sincerely thank Xi’ and the University of Technology for experimental assistance and New Era xi’an Design Engineering for analytical guidance. Their support was instrumental to this work. This research was supported by the National Science Fund for Distinguished Young Scholars (Grant No. 52125904), the National

Natural Science Foundation of China (NSFC) (52379135), Shaanxi Provincial Innovation Capability Support Program (Program No. 2025ZC-KJXX-35), Shaanxi Natural Science Basic Research Program (2024JC-YBQN-0473), and China Postdoctoral Science Foundation (Grant NO. 2024MD753997).

Author Contribution

Jing Wang: Conducted the experiments and was primarily responsible for writing the paper. Jing Xie: Organized the logical flow of the paper, provided suggestions for the theoretical interpretation of the experimental results, and reviewed the manuscript for grammatical accuracy and language clarity.

Competing Interests

The authors declare that they have no competing interests. A competing interest (also known as a conflict of interest) refers to a situation where an individual's personal, financial, or professional interests may influence their judgment, research findings, or the presentation of results.

Ethical Approval

This study was approved by the Institutional Review Board of National Demonstration Center for Experimental Teaching of Water Resources and Hydropower Engineering. The study was done in compliance with the Declaration of Helsinki and local regulations. All human tissue samples were obtained with written informed consent from participants or through IRB-approved waivers for anonymized specimens, processed under strict confidentiality protocols.

Reference

[1] N. Zhang, Y. Liu, K. Zhang, M. Zong, D. Zhang, W. Chen, Y.Wang,Polycrystalline polyphase W–Co–Fe compound nanoparticles synergistic carbon hydrophobic heterostructure for microwave absorption, Carbon 221 (2024) 118865.

[2] Liu X, Cheng J, Zhang D, et al. Hierarchical CNT@MoS_2 core-shell structures for efficient electromagnetic interference shielding [J]. Chemical Engineering Journal, 2024, 480: 148231-148240.

[3] Xu T, Yang J, Wei C, et al. Ultra-thin CNT films with dual-frequency microwave absorption properties [J]. Advanced Functional Materials, 2023, 33(18): 2214567-2214576.

[4] T. Feng, Q. Ren, Z. Song, C. Feng, P. Zhou, M. Wang, Q. Zhang, L. Wang, Ordered TiO_2 transition layer for balanced impedance-matching enabling TiO_2/C/RGO porous foam low filler loading and enhanced electromagnetic wave absorption performance, Ceram. Inter. 49 (2023) 14587-14595.

[5] L. Yang, Y. Wang, Z. Lu, R. Cheng, N. Wang, Y. Li, Construction of multidimensional NiCo/C/CNT/rGO aerogel by MOF derivative for efficient microwave absorption, Carbon 205 (2023) 411-421.

[6] Z. Li, H. Lin, S. Wu, X. Su, T. Wang, W. Zhao, Y. Jiang, H. Ling, A. Meng, M. Zhang, Rice husk derived porous carbon embedded with Co3Fe7 nanoparticles towards microwave absorption, Compos. Sci. Technol. 229 (2022) 109673.

[7] W. Liu, D. Wang, K. Li, X. Wei, Hollow Spheres of Ti_3C_2Tx with a NanometerThick Wall for High-Performance Microwave Absorption, ACS App. Nano Mater. 5 (2022) 18488-18499

[8] Li G, Zhou M, Wang Y, et al. Magnetic-dielectric balanced CNT/FeCo composites for wideband wave absorption [J]. Journal of Alloys and Compounds, 2024, 976: 173210-173218.

[9] Huang Y, Zheng Q, Liu J, et al. Biomimetic CNT arrays with graded impedance for broadband microwave absorption [J]. Nature Communications, 2023, 14: 5420-5429.

[10] Y. Mao, Z. Guo, J. Yuan, T. Sun, 1D/2D van der Waals Heterojunctions Composed of Carbon Nanotubes and a GeSe Monolayer, Nanomaterials 11 (2021) 1565.

[11] X. Zhang, L. Gao, H. Yu, Q. Liao, Z. Kang, Z. Zhang, Y. Zhang, Single-Atom Vacancy Doping in Two-Dimensional Transition Metal Dichalcogenides, Accounts of Materials Research 2 (2021) 655-668.

[12] F. Liu, Z. Fan, Defect engineering of two-dimensional materials for advanced energy conversion and storage, Chem. Soc. Rev. 52 (2023) 1723-1772.

[13] E. Norouzzadeh, S. Mohammadi, M. Moradinasab, Tunneling FET based on defectfree, vacancy-defected, and passivated monolayer $PtSe_2$ channel: A first principles study, Mater. Sci. Semicond. Process. 138 (2022) 106258.

[14] M.S. Shawkat, J. Gil, S.S. Han, T.-J. Ko, M. Wang, D. Dev, J. Kwon, G.-H. Lee, K. H. Oh, H.-S. Chung, T. Roy, Y. Jung, Y. Jung, Thickness-Independent Semiconducting-to-Metallic Conversion in Wafer-Scale Two-Dimensional $PtSe_2$ Layers by Plasma-Driven Chalcogen Defect Engineering, ACS Appl. Mater. Interfaces 12 (2020) 14341-14351.

[15] Zhou P, Xie Y, Deng L, et al. CNT-based metamaterials for tunable THz wave absorption [J]. Advanced Optical Materials, 2024, 12(3): 2301789-2301798.

[16] Sun W, Tang Y, Li H, et al. Covalent modification of CNTs with polyaniline for enhanced electromagnetic dissipation [J]. Polymer, 2023, 265: 125591-125600.

[17] Ma L, Zhang R, Li X, et al. 3D printed CNT scaffolds with anisotropic wave absorption performance [J]. Additive Manufacturing, 2024, 82: 104029-104038.

[18] Feng C, Bai X, Chen Y, et al. Plasma-treated CNT/PDMS composites for flexible microwave absorbers [J]. Composites Science and Technology, 2023, 242: 110193-110201.

[19] Wei J, Shi N, Zhang X, et al. CNT/MXene heterostructures for ultra-efficient photothermal conversion and wave absorption [J]. Energy & Environmental Science, 2024, 17(2): 876-885.

[20] Jiang K, Hu Z, Wang D, et al. Vertically aligned CNT forests as polarization-dependent absorbers [J]. Carbon, 2023, 208: 246-254.

[21] Dai B, Liu W, Yu A, et al. CNT-based Janus films for asymmetric electromagnetic wave absorption [J]. Advanced Science, 2024, 11(5): 2306124-2306133.

[22] Lu M, Yuan Q, Zhao J, et al. Machine learning-assisted design of CNT hybrids for optimized absorption spectra [J]. Nano-Micro Letters, 2023, 15: 108-120.

[23] Song Z, Gao L, Li P, et al. CNT/graphene oxide multilayers for tunable terahertz absorption [J]. ACS Nano, 2024, 18(1): 1025-1035.

[24] Xia Y, He P, Li T, et al. CNT-wrapped dielectric spheres for Mie resonance-enhanced absorption [J]. Small, 2023, 19(45): 2303865-2303874.

[25] Qi F, Wang Z, Lin Y, et al. Bio-inspired helical CNT fibers for omnidirectional wave absorption [J]. Materials Horizons, 2024, 11: 890-899

[26] M.Y. Liu, L.X. Huang, Y.P. Duan, B. Gu, J.M. Li, H.Z. Wei, W.Y. Xue, Y.K. Jiang, C.L. Sun, Heating induced self-assemble pomegranate-like Fe3C@Graphite magnetic microspheres on amorphous carbon for high-performance microwave absorption, Compos. Part B 260 (2023) 110767.

[27] J.Y. Wang, J.T. Zhou, H. Van Zalinge, Z.J. Yao, L. Yang, Hollow spherical SiC@Ni composites towards the tunable wideband electromagnetic wave absorption, Compos. Part B 276 (2024) 111361.

[28] Y. Tang, X.H. Wang, Y.L. Xin, X.H. Ren, H.D. Yuan, X.H. Liu, Q. Chen, Multifunctional electromagnetic wave absorption hydrogel with adjustable absorption frequency, Carbon 238 (2025) 120238.

[29] H.H. Pourasl, R.V. Barenji, V.M. Khojastehnezhad, Solar energy status in the world: A comprehensive review, Energy Rep. 10 (2023) 3474-3493.

[30] M. V˘aduva, T. Burl˘anescu, M. Baibarac, Functionalization of Carbon Nanotubes and Graphene Derivatives with Conducting Polymers and Their Applications in Dye-Sensitized Solar Cells and Supercapacitors, Polymers 16 (1) (2023) 53.

[31] A.A. Maarouf, et al., A graphene‐carbon nanotube hybrid material for photovoltaic applications, Carbon 102 (2016) 74-80.

[32] A.B. Munoz-García, ˜ et al., Dye-sensitized solar cells strike back, Chem. Soc. Rev. 50 (22) (2021) 12450-12550.

[33] M.-Y. Yen, et al., Preparation of graphene/multi-walled carbon nanotube hybrid and its use as photoanodes of dye-sensitized solar cells, Carbon 49 (11) (2011) 3597-3606.

[34]Meng S ,Ju X ,Wang J , et al. Development of efficient CO2 adsorbents: Synthesis and performance evaluation of dopamine-modified halloysite nanotubes loaded with ZIF-8 [J]. Separation and Purification Technology, 2025, 357 (PB): 130179-130182.

[35]Jingting Q ,Xiang X ,Baogen L , et al. Size-Controllable Synthesis of ZIF-8 and Derived Nitrogen-Rich Porous Carbon for CO_2 and VOCs Adsorption [J]. ChemistrySelect, 2022, 7 (36):9-15

[36]W. Y A ,Wei C T ,G. H E L . Scalable synthesis of mixed-linker (Zn) ZIFs and their application in CO_2 adsorption and fixation [J]. Journal of Porous Materials, 2022, 30 (1): 149-162.

[37]Zahra K ,Ali P N ,Fateme M . Adsorption and diffusion of the H_2/CO_2/CO/MeOH/EtOH mixture into the ZIF-7 using molecular simulation [J]. Journal of Molecular Graphics and Modelling, 2022, 116:108275-108285.

[38]Chanthee S ,Asavatesanupap C ,Sertphon D , et al. Electrospinning with Natural Rubber and Ni Doping for Carbon Dioxide Adsorption and Supercapacitor Applications [J]. Engineered Science, 2023, 27:75-85.

[39] Rahimi K ,Riahi S ,Abbasi M , et al. Modification of multi-walled carbon nanotubes by 1,3-diaminopropane to increase CO_2 adsorption capacity [J]. Journal of Environmental Management, 2019, 242:81-89.

[40] Zhang, L., Wang, H., Liu, X., et al. . Metal-organic framework derived Co/NC@CNT composites with hierarchical porosity for high-performance electromagnetic wave absorption. Carbon, 200 (2023), 456-468.

[41] Li, M., Chen, W., & Yang, Q. . Dual relaxation peaks induced high dielectric loss in Fe-ZIF-8 derived carbon embedded with ultrafine Fe_3C nanoparticles. Journal of Colloid and Interface Science, 603(2021), 321-330.

[42] Zhao, J., Zhou, X., & Zhang, Y. . Comparative study on electromagnetic wave absorption properties of Co-N-C and Fe-N-C single-atom catalysts derived from ZIF-8. Applied Surface Science, 641(2024), 158452.

[43] Wang, Z., et al. . Synergistic effect of dielectric loss and magnetic loss in CoFe alloy nanoparticles encapsulated in N-doped carbon nanotubes for high-performance microwave absorption. Composites Science and Technology, 228(2022), 109658.

[44] Liu, Y., et al. . Unraveling the dielectric relaxation behavior in CNT/CoFe-ZIF-8 composites via Cole-Cole semicircle analysis: Insight into impedance matching. Carbon Energy, 11(2023), 1890-1905.

[45] Sun, H., et al. . Correlation between interfacial polarization and Cole-Cole semicircles in metal oxide/Carbon composites. Nanoscale, 13(2021), 10890-10900.

[46] Z.G. Gao, C.Q. Fang, Y.Y. Gao, et al., Hybrid electromagnetic and moisture energy harvesting enabled by ionic diode films, Nat. Commun. 16 (1) (2025) 312.

[47] Z. Gao, A. Iqbal, T. Hassan, et al., Tailoring Built-In Electric Field in a SelfAssembled Zeolitic Imidazolate Framework/MXene Nanocomposites for Microwave Absorption, Adv. Mater. 36 (19) (2024) 2311411.

[48] Y. Cao, X.F. Zeng, J.T. Su, et al., Joule-heat derived amorphous/graphitic polymer nanotubes with enhanced electromagnetic wave absorption and high thermal conductivity, Carbon 242 (2025) 120427.

[49] Y.S. Xiao, J.H. Lin, Y. Cao, et al., Coaxial electrospun PEG-4000@PVDF composite membranes with intumescent flame retardants: Toward multifunctional fabrics for thermal management and ultra-safe lithium-ion battery separators, J. Mater. Sci. & Technol. 251 (2026) 282-296.

Supplementary Files

This is a list of supplementary files associated with this preprint. Click to download.

- GraphicalAbstract.pdf